Cell type-dependent differential activation of ERK by oncogenic KRAS or BRAF in the mouse intestinal epithelium

Raphael Brandt[1], Florian Uhlitz[2], Pamela Riemer[1,3], Claudia Giesecke[4], Silvia Schulze[1], Ismail Amr El-Shimy[2], Beatrix Fauler[5], Thorsten Mielke[5], Norbert Mages[5], Bernhard G Herrmann[5], Christine Sers[1,3], Nils Blüthgen[1,2,3], and Markus Morkel[1,3,*]

[1] Laboratory of Molecular Tumor Pathology, Institute of Pathology, Charité Universitätsmedizin Berlin, Chariteplatz 1, 10117 Berlin, Germany

[2] IRI Life Sciences, Humboldt University Berlin, Philippstrasse 13, 10115 Berlin, Germany

[3] German Cancer Consortium (DKTK), German Cancer Research Center (DKFZ), 69120 Heidelberg, Germany

[4] Department of Cell Biology, German Rheumatism Research Center, Leibniz Institute, Berlin, Germany.

[5] Max Planck Institute for Molecular Genetics, Ihnestr. 73, 14195 Berlin, Germany

[*]corresponding author: markus.morkel@charite.de, Tel: ++49-30-450 536 107, Fax: ++49 - 30-450 536 909, ORCID-id: 0000-0002-2553-9999

Short title: $KRAS^{G12V}$ and $BRAF^{V600E}$ in intestinal organoids

Key words: Organotypic Cell Culture, MAPK, Wnt/beta-Catenin, Cell Differentiation, Cancer Development

Abstract

Mutations activating the KRAS GTPase or the BRAF kinase are frequent in colorectal cancer. Here, we use inducible transgenic expression of $KRAS^{G12V}$ or $BRAF^{V600E}$ in intestinal organoids of mice to investigate oncogenic signal transduction in the mitogen-activated protein kinase (MAPK) cascade with cellular resolution. Using phospho-protein, reporter, and single cell transcriptome analyses, we found that $BRAF^{V600E}$ triggered high ERK activity and downstream gene expression in all intestinal cell types. Induction of $BRAF^{V600E}$ resulted in rapid epithelial disorganisation followed by organoid disintegration, providing evidence for an upper limit of tolerable MAPK activity in the intestinal epithelium. In contrast, transgenic expression of $KRAS^{G12V}$ activated ERK to a lesser extent and in a cell type-specific pattern. Single cell RNA sequencing defined three intestinal cell types capable of activating ERK: undifferentiated crypt cells, Paneth cells and a minority population of late-stage enterocytes. Yet, in most enterocytes ERK was not activated by EGF in the medium or induction of oncogenic $KRAS^{G12V}$. Colorectal cancer cell lines also differed in their abilities to activate ERK in response to $KRAS^{G12V}$. Furthermore, we found that Wnt/β-Catenin amplified ERK phosphorylation in the normal intestine and $KRAS^{G12V}$ could maintain proliferation only in adenomatous cells forming after β-Catenin activation. These findings may explain why activation of Wnt signalling precedes KRAS mutations in the classical CRC progression pathway. Our experiments highlight key differences between MAPK activity elicited by the BRAF or KRAS oncogenes in colorectal cancer and find unexpected functional heterogeneity in a signalling pathway with fundamental relevance for cancer therapy.

Introduction

Multiple signalling pathways, including the Wnt/β-Catenin and the mitogen-activated protein kinase (MAPK) cascades, form a signalling network in cells of the intestinal epithelium [1]. Collectively, activities within the signalling network control cellular turnover, that is, stem cell maintenance, cell proliferation, differentiation into absorptive enterocyte and secretory cell lineages, and apoptosis. Wnt/β-Catenin and MAPK activities are regionalized within the folded single-layered intestinal epithelium. Both are high in crypt bases harbouring stem cells and low in villus areas containing differentiated enterocytes.

The MAPK module transduces signals downstream of receptor tyrosine kinases, such as EGFR, and RAS family GTPases. MAPK comprises of three consecutively activated kinases, namely RAF, MEK and ERK. Upon activation, ERK can phosphorylate and activate a series of transcription factors orchestrating a complex cellular response that often is pro-proliferative [2]. In the normal intestine, EGFR-RAS-MAPK is activated by ligands from the crypt microenvironment, which are secreted by e.g. epithelial Paneth cells of the small intestine, Reg4+ secretory niche cells of the large intestine, or adjacent fibroblasts [3,4]. In colorectal cancer (CRC), MAPK activity is thought to be more cell-autonomous due to oncogenic mutations activating KRAS (in 40% of CRCs) or NRAS (5% of CRCs) [5] or BRAF (10% of CRCs) [6], or by *de novo* expression of EGFR ligands such as amphiregulin [7]. Activity of the RAS-MAPK signal transduction module is a main determinant of cancer development and therapy response [5,6,8].

Recent studies suggest that the relationship between MAPK-activating mutations, MAPK signal transduction and phenotypic outcome in CRC is complex: firstly, mutations in KRAS and BRAF are associated with distinct CRC development routes: KRAS, but not BRAF, mutations frequently occur as secondary events after mutations activating Wnt/β-Catenin in the conventional CRC progression sequence [9,10]. Conversely, BRAF, but less frequently KRAS, mutations precede upregulation of Wnt/β-Catenin in the alternative serrated progression route [11,12]. The observed disequilibrium between KRAS and BRAF mutations in the conventional versus serrated pathways of CRC evolution suggest the existence of functional differences, resulting in distinctive effects on clinical course and treatment efficacy [13].

Secondly, MAPK signal transduction appears to be heterogeneous in genetically identical CRC cells. Cells at the invasive front frequently exhibited more MAPK activity compared to cells in central areas of the same cancer, as judged by phosphorylation of ERK (p-ERK), and CRCs with activating KRAS mutations retained regulation of MAPK [14]. Previous studies already showed heterogeneous Wnt/β-Catenin activity in cancer specimens, suggesting a more general paradigm of graded pathway

activities in CRC [15]. Furthermore, CRC cells exhibit functional differences within a cancer. Differentiation gradients in CRC appear related to differentiation trajectories of normal intestinal cells, with stem cells at the apex of the hierarchy [16–19]. CRC subtypes can share similarities with cell types of the normal crypt, such as stem cells, enterocytes or secretory cells in bulk cell analysis [20]. Finally, because of variable signal transduction and differentiation states, genetically identical CRC clones exhibit variable proliferative potential and therapeutic response [21].

Experimental techniques with cellular resolution, ranging from fluorescent reporters [22] to single-cell transcriptome analyses [23,24] hold the promise to disentangle the relationship between oncogenes, cell differentiation states and cell signal transduction while taking into account cellular heterogeneity. Here, we ask whether oncogenic KRAS or BRAF, representing the most common alterations in the MAPK pathway in CRC, show cell-to-cell heterogeneity in their activities. For this, we use organoid cultures that can be efficiently manipulated and which maintain the cell hierarchy of the tissue *in vitro* [25]. In these organoids, we express transgenes encoding $BRAF^{V600E}$, $KRAS^{G12V}$ and/or stabilized β-Catenin (β-$Catenin^{stab}$), along with the fluorescent marker tdTomato. We assess the immediate impact of the oncogenes on cell signal transduction, gene expression programs and phenotypic outcome using an ERK-dependent fluorescent reporter and single cell RNA sequencing. We discover strong functional differences between the BRAF and KRAS oncogenes and find that signal transduction by KRAS is cell type-specific.

Results

BRAF^{V600E}, but not KRAS^{G12V}, induces high levels of MAPK activity and epithelial disorganisation in intestinal organoids

To study direct effects of the KRAS^{G12V} and BRAF^{V600E} oncoproteins on cells of the intestinal epithelium, we engineered transgenic mice carrying doxycycline-inducible single copy transgenes in the Gt(ROSA26)Sor locus [26,27]. For the present study, we employed lines with transgenes encoding the red fluorescent marker tdTomato linked by a self-cleaving p2A peptide to BRAF^{V600E}, KRAS^{G12V}, or stabilized β-Catenin (Fig. 1A), alone and in combination, and tdTomato linked to firefly luciferase (FLUC) as a control.

We initiated organoid cultures by embedding intestinal crypts from FLUC-, KRAS^{G12V}-, and BRAF^{V600E}-inducible mice into extracellular matrix, as described before [25]. BRAF^{V600E} induced irreversible disintegration of organoids within 1-2 days, whereas transgenic KRAS^{G12V} or the FLUC control protein were well tolerated, even after several passages, when we initiated oncoprotein production by adding doxycycline to the culture media (Fig. 1B). To examine whether the BRAF oncogene has detrimental effects on the epithelium beyond the previously reported loss of stem cells [27,28], we examined histology at ultrastructural level of the induced organoids using transmission electron microscopy (Fig. 1C). We found that control and KRAS^{G12V}-induced organoids show the expected tissue structure, that is, a single-layered polarized epithelium with continuous apical and basal surfaces as well as a brush border at the apical side. Desmosomes, providing lateral cell adhesion, were clearly visible. We frequently observed intercellular vacuoles, which have previously been attributed to osmotic stress during fixation of organoids [25]. In contrast, BRAF^{V600E}-induced organoids displayed a continuous basal surface, whereas the apical side was grossly distorted, although it contained a brush border as evidence of polarisation. Nuclei were pleomorphic and no longer lined up basally but were scattered at different positions. Cells were still attached to each other by desmosome bridges, indicating that the ongoing epithelial disorganisation was taking place in the presence of lateral cell adhesion.

To ascertain whether the epithelial disorganisation provoked by BRAF^{V600E} was correlated with MAPK activity, we measured phosphorylation of ERK. We found that induction of BRAF^{V600E}, but not KRAS^{G12V}, resulted in high phosphorylation levels of ERK in intestinal organoids, as determined by capillary protein analysis (Fig. 1D). BRAF^{V600E}-induced organoid disintegration could be counteracted by inhibition of the BRAF-downstream MEK and ERK kinases using AZD6244/Selumetinib [29] and BVD-523/Ulixertinib [30], respectively, but not by inhibition of the upstream EGFR tyrosine kinase receptor family using AZD8931/Sapitinib [31] (Fig. 1E), showing that the induced phenotype is due to

1 excessive MAPK activity. Indeed, only 24 h of BRAF^{V600E} induction activated almost all direct MAPK
2 target genes [32], whereas conditional expression of KRAS^{G12V} had no obvious effect on bulk organoid
3 transcription (Supplementary Fig. 1).

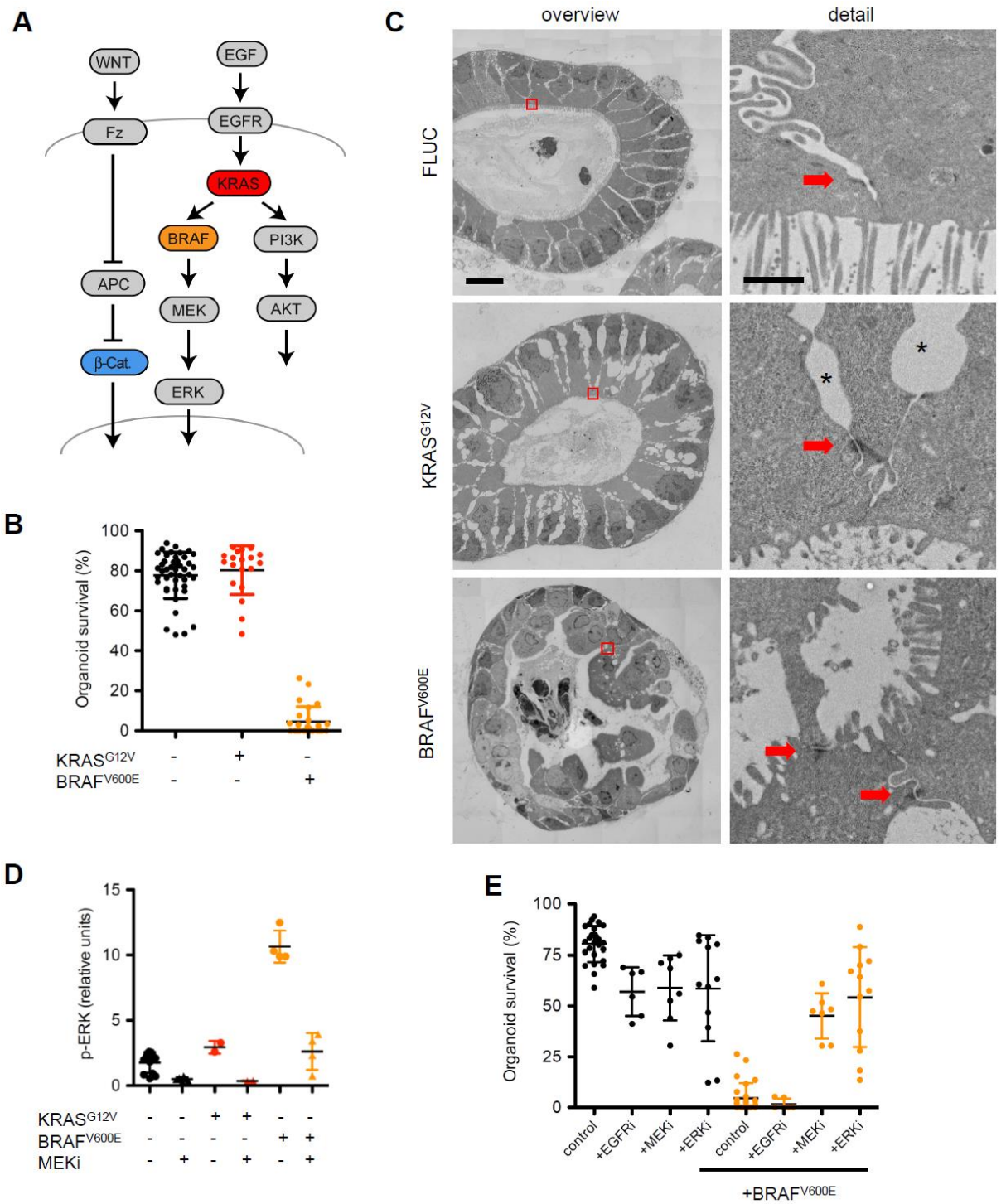

4

5 **Figure 1: Transgenic induction of BRAF^{V600E}, but not KRAS^{G12V} disrupts intestinal organoids due to**
6 **high MAPK activity** A) Simplified representation of the MAPK and β-Catenin pathways, indicating the
7 relative positions of the KRAS, BRAF and β-Catenin proto-oncogenes. B) Organoid survival 4 d after
8 induction of oncogenic KRAS^{G12V} or BRAF^{V600E}. Organoids are counted 1 d after passaging, and

fractions of surviving organoids were calculated at day 4. Organoid survival was judged by presence of crypt domains and a continuous basal surface. Control organoids comprise of mixed non-induced cultures of the $KRAS^{G12V}$ or $BRAF^{V600E}$ lines. C) Electron microscopy reveals epithelial damage after $BRAF^{V600E}$ induction. Images of the intestinal organoid epithelium, 24 h after induction of control, $KRAS^{G12V}$ or $BRAFV^{600E}$ transgenes. Detailed views (right) represent a zoom into areas marked by red boxes in the overviews (left). Detailed views show apical surfaces of adjacent enterocytes with brush border. Red arrows mark desmosomes. Intercellular vacuoles, most visible in the $KRAS^{G12V}$ model (marked by *) are likely fixation-induced artefacts, see ref. [25]. Scale bars are 10 µm in the overview panels and 1 µm in the detailled view panels. D) phospho-ERK quantification in organoids, 24 h after induction of control, BRAF or KRAS transgenes, using a capillary protein analysis. E) Quantification of organoid survival 4 d after inhibition of EGFR, MEK, ERK and/or induction of oncogenic BRAF, as in panel B).

Single cell RNA sequencing reveals disruption of intestinal differentiation trajectories by $BRAF^{V600E}$

To uncover potential cellular heterogeneity in the response to the oncogenes, we performed single cell transcriptome analyses. We induced FLUC control, $BRAF^{V600E}$ and $KRAS^{G12V}$-transgenic organoids for 24 h, prepared single cell suspensions, and stained them with a fluorescent antibody against the crypt cell marker CD44 [33], and with a fluorescent dye to eliminate dead cells. We next sorted single live and transgene-expressing organoid cells into two 96-well plates for RNA sequencing. We acquired samples of CD44-high crypt and CD44-low villus cells. In total, we obtained transcriptomes of 167 cells with >1000 detected genes per cell that were used for further analysis. Single cell transcriptomes were assigned to six interconnected clusters with help of k-means clustering and visualised in a t-SNE-based representation (Fig. 2A). Mapping of signature genes for intestinal stem cells (ISCs), proliferative TA cells, differentiated enterocytes [34] and secretory Paneth cells [35] (Fig. 2B), and the CD44 status as inferred from flow cytometry (Fig. 2C) confirmed the calculated differentiation trajectories (shown as branched grey overlay in Fig. 2A; cluster 1 was assigned starting cluster): undifferentiated CD44-high ISC and TA cell signature genes were enriched in clusters 1 and 2 while Paneth cell marker genes were highest in cluster 2, indicating the route for secretory crypt cells differentiation; expression of enterocyte signature genes increased gradually in clusters 3-5, marking the CD44-low absorptive lineage.

We next considered the distribution of cells expressing specific transgenes: FLUC control and $KRAS^{G12V}$-expressing cells intermingled throughout the clusters 1-5 of the normal cell differentiation

trajectories. BRAF^{V600E}-expressing cells were in contrast depleted from the central clusters 2-4, but formed the outsider cluster 6, composed entirely of BRAF-induced cells. BRAF^{V600E}-positive cells in cluster 6 uniformly expressed high levels of ERK target genes, regardless of whether they were sorted as CD44-high or CD44-low (Fig. 2C). Cluster 6 also had high expression of *Anxa10*, which has been identified as a marker for BRAF-positive serrated adenoma [36](Supplementary Fig. 2). The single cell analysis thus shows that BRAF^{V600E} imposes a specific gene expression program onto intestinal cells, independent of their prior differentiation state.

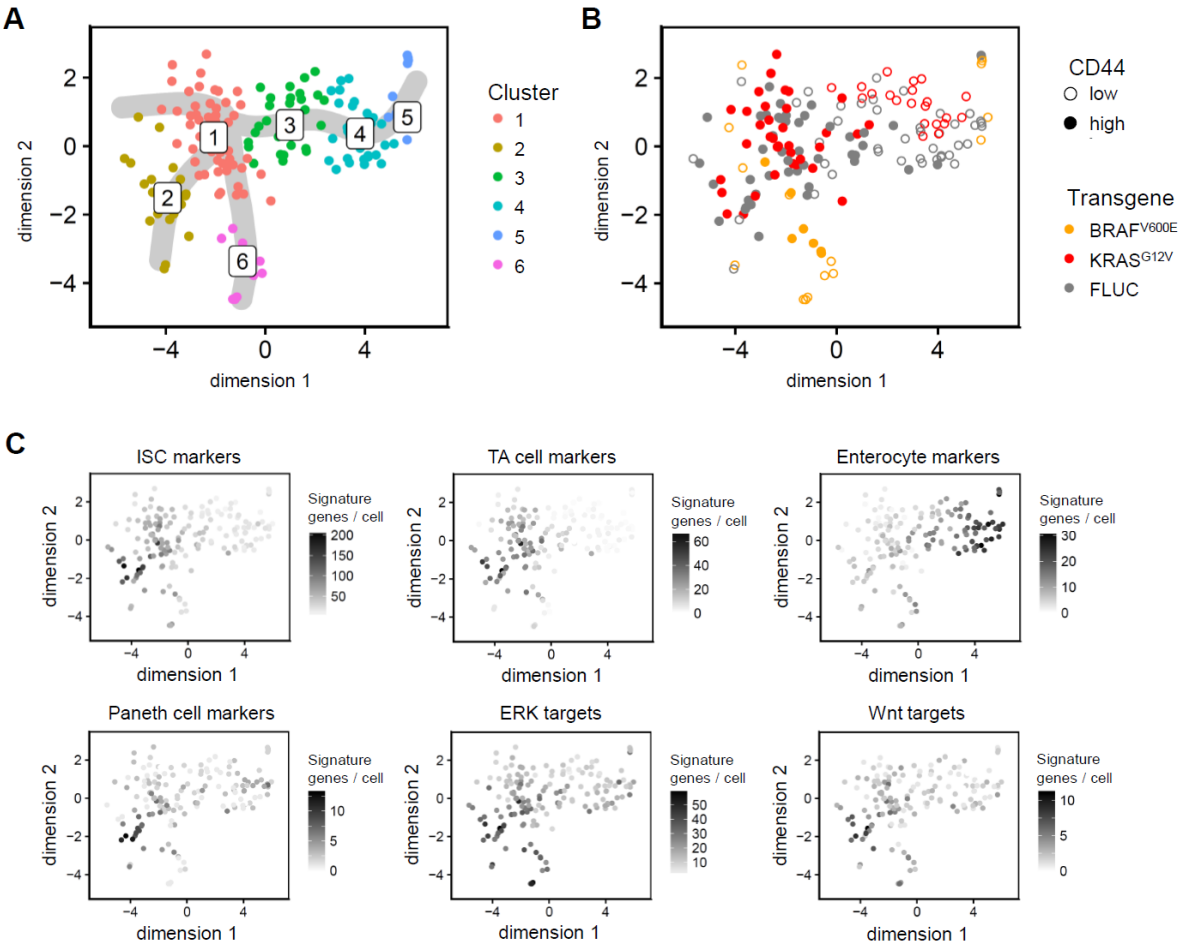

Figure 2: Single cell RNA sequencing of transgenic organoids reveals differential effects of BRAF^{V600E} or KRAS^{G12V} on gene expression and intestinal cell hierarchies. t-SNE visualisations and clustering of organoid single cell transcriptomes clustered with k-means, 24 h after induction of FLUC control, BRAF^{V600E} or KRAS^{G12V} transgenes. A) Transcriptomes are colour-coded for six clusters, and inferred differentiation trajectories are shown as overlay. B) Colour-code for transgene and CD44 positivity, as inferred from flow cytometry. C) Mapping of cell- and pathway-specific differentiation signatures. Numbers of reads mapping with signature genes are given per single cell transcriptome.

ERK-dependent reporter activity and single cell analyses identify KRAS^{G12V}-responsive intestinal cells

Since mutant KRAS is one of the most frequent oncogenes in colon cancer, we were intrigued by the absence of KRAS^{G12V}-induced MAPK activity, phenotypes, or gene expression changes in our previous assays. We hypothesized that its activity could be weak and restricted to specific cell types in the normal intestine. To visualize ERK activity with single cell resolution in organoids, we employed the Fra-1-based integrative reporter of ERK (FIRE) that translates ERK kinase activity into stability of a nuclear yellow-green venus fluorescent protein (Fig. 3A) [22]. FIRE fluorescence in organoids cultured in normal growth medium containing EGF was strong in crypt bases, whereas differentiated villus tissue was largely FIRE-negative (Fig. 2B). In the absence of EGF from the medium, ERK activity in the crypt base persisted, likely due to autocrine and paracrine signals from EGF-producing Paneth cells [4].

We next conditionally expressed the FLUC control, KRAS^{G12V}, or BRAF^{V600E}-encoding transgenes in FIRE-transfected organoids (Fig. 3C). Transgene induction was often variable, as inferred by tdTomato fluorescence, allowing to compare individual tdTomato-positive cells with transgene-negative neighbouring tissue. tdTomato-FLUC control transgene expression had no influence on FIRE activity. In contrast, expression of KRAS^{G12V} resulted in increased FIRE signals in crypt cells, which consistently displayed stronger reporter activity compared to adjacent KRAS^{G12V}-negative cells. Surprisingly, a large majority of villus cells remained FIRE negative, despite strong KRAS^{G12V} positivity, as inferred from tdTomato fluorescence. We confirmed the differential signal transduction from KRAS^{G12V} to ERK using phospho-ERK immunohistochemistry (Fig. 3D). In line with our FIRE reporter data, p-ERK-positive cells were largely absent in the central differentiated (Ki67-negative) villus areas of organoids, despite strong tdTomato-KRAS^{G12V} positivity. Taken together, our results show that ERK activity in differentiated villus epithelial cells can neither be induced by EGF in the medium nor by induction of oncogenic KRAS^{G12V}. However, when we induced BRAF^{V600E}, we found widespread and strong FIRE signals across the complete organoid (Fig. 3C). This suggests a strict and cell-type specific control of signal transduction by oncogenic KRAS, but not BRAF in intestinal epithelial cells.

Since FIRE fluorescence was detected in cells responsive to KRAS^{G12V}, we next used the reporter to assist selection of cells for single cell sequencing. Our aim was to define cell types with high ERK activity, either in response to KRAS^{G12V} or as part of the normal cell hierarchy. For this, we induced organoids with the integrated ERK reporter for KRAS^{G12V} or FLUC, prepared single cell suspensions and sorted cells by FACS into 96-well plates for transcriptome analysis (Supplementary Fig. 3). We focussed on single cells with high transgene (tdTomato) signal and either strong or weak FIRE (venus) fluorescence (Fig. 4A). In total, we obtained 197 single cell transcriptomes. K-means clustering into 8

groups and t-SNE-based visualisation (Fig. 4B, C) revealed the cell type distribution. We found gene expression patterns characteristic for immature and secretory cells in clusters 1-4. Cluster 1 was enriched for ISC and TA marker genes, whereas clusters 2-4 were defined by Paneth cell signature genes (Fig 4D; Supplementary Fig. 4). Cluster 2 was enriched for the Paneth cell markers *Lyz1* encoding Lysozyme [37] and several genes encoding Defensins, while other cluster-defining genes such as *Mptx1* and *Agr2* in cluster 4 hint at a high degree of Paneth cell heterogeneity. Clusters 5-8 formed a differentiation trajectory for absorptive cells, with *Ifabp1* as the top defining genes for clusters 5-7 (Supplementary Fig. 4)

Using this information, we assessed the distribution of transcriptomes derived from KRAS^{G12V}-induced FIRE-high cells (Fig. 4C, D). These were confined to distinct aggregates encompassing the ISC/TA cell zone of cluster 1, as well as transcriptomes inhabiting the outer right rim of the tSNE representation that we above assigned to be derived from late-stage enterocytes and Paneth cells. Immunofluorescence microscopy using the Paneth cell marker Lysozyme confirmed high FIRE activity in this cell type after KRAS^{G12V} induction (Supplementary Fig. 5). In contrast, a central area of the tSNE plot encompassing the largest clusters 5 and 6 of bulk enterocytes was almost devoid of KRAS^{G12}-producing FIRE-high cells but harboured many KRAS^{G12V}/FIRE-low cells, confirming that enterocytes cannot activate ERK, even when expressing oncogenic KRAS^{G12V}.

Inspection of the MAPK-driven ERK target signature in the clustered transcriptomes revealed a complex picture (Fig.4D): KRAS^{G12V}/FIRE-high cell transcriptomes of cluster 1 displayed low expression of ERK signature genes, probably due to quickly diminishing ERK activity and transcription in committed TA cells that transiently remain positive for FIRE, due to its integrative fluorescence reporting characteristics [22]. In contrast, multiple FIRE-positive Paneth cells of clusters 2-4 and enterocytes at the edge of clusters 7 and 8 displayed had ERK activity, as inferred from ERK target gene expression. We hypothesize that the burst of ERK activity in late-stage enterocytes is directly or indirectly related to the apoptotic process at the end of their life span. Indeed, a previous publication has identified a role for ERK signals in cells neighbouring an apoptotic enterocyte [38]. It remains to be tested whether the burst of ERK activity in some late-stage enterocytes is amplified by KRAS^{G12V}; we found that isolated FIRE-positive cells were present in organoid villus domains regardless of KRAS^{G12V} induction (compare cells marked with asterisks in Figs. 3B and 3C). Taken together, our single cell RNA and reporter analyses show that crypt cells, encompassing ISC/TA cells and Paneth cells, can activate ERK as a response to oncogenic KRAS^{G12V}. In contrast, enterocytes were unable to activate ERK despite EGF in the medium or expression of KRAS^{G12V}.

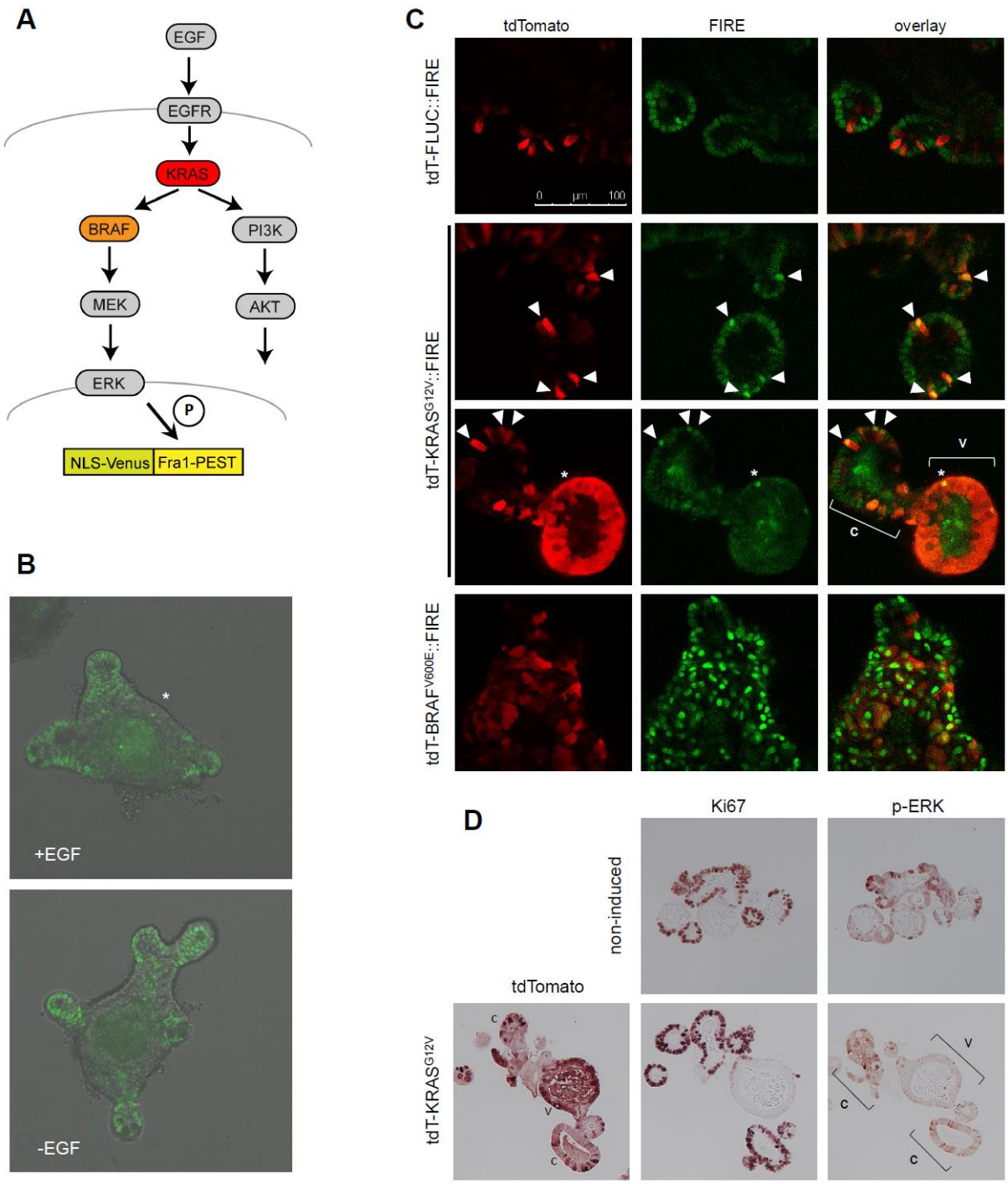

Figure 3: Visualisation of ERK activity by FIRE reveals KRAS^{G12V}-responsive cells. A) Schematic representation of MAPK pathway and reporter B) FIRE activity in intestinal organoids, in the presence and absence of EGF in the culture medium, as indicated. Asterisk marks isolated FIRE high villus cell. C) Fluorescence microscopy images showing transgene expression (red), FIRE activity (green), and overlays in intestinal organoids, taken 2 d (FLUC, KRAS) or 1 d (BRAF) after transgene induction. Arrow heads mark KRAS^{G12V}/FIRE high crypt cells, asterisk marks FIRE high villus cell, c and v demarcate crypt and villus areas, respectively. D) immunohistochemistry of tdTomato, Ki67 and p-ERK in intestinal organoids, as indicated. c and v mark crypt and villus areas, respectively.

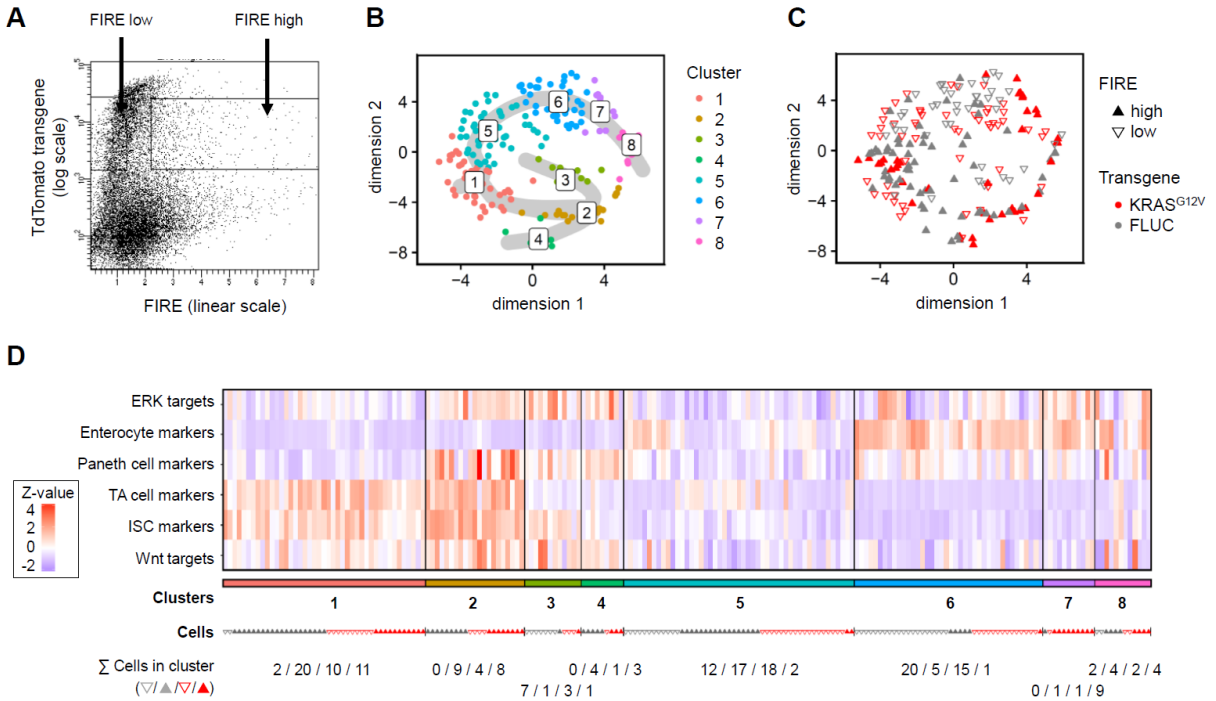

Figure 4: Single cell RNA sequencing of FIRE transgenic organoids reveals populations of KRAS^{G12V}-responsive and -unresponsive cells A) Diagram of fluorescence-activated cell sort windows for FIRE low and high cells. B) t-SNE visualisation colour-coded for eight clusters identified with k-means clustering. Inferred differentiation trajectories, starting in cluster 1, are shown as overlay. C) tSNE visualisation displaying colour-codes for transgene and FIRE positivity, as inferred from flow cytometry. Filled upward-pointing triangles: FIRE-high; outlined downward-pointing triangles: FIRE-low. Red: KRAS^{G12V}; grey: FLUC. D) Heat map of z-transformed signature scores per cell for cluster cell type identification. Signature scores correspond to number of expressed signature genes per cell normalised to gene detection rate and signature length. Blue: low target gene signature abundance; Red: high target gene signature abundance. Cluster colour codes, transgene and FIRE positivity codes, and cell numbers are given below the heat map.

β-Catenin interacts with KRAS^{G12V} in regulating ERK phosphorylation and EGFR signal autonomy

We asked whether Wnt/β-Catenin activity may enable the cellular ERK response, because ERK-responsive crypt cell types, as defined above, are known to have high Wnt/β-Catenin activity, whereas unresponsive enterocytes have low Wnt/β -Catenin activity [39] (see also Wnt target gene activity in Fig. 4D). Furthermore, activating KRAS mutations usually follow mutations activating the Wnt/β-Catenin pathway in conventional CRC progression [9]. We first analysed ERK phosphorylation

in intestines of induced transgenic mice carrying single or combined transgenes encoding stabilized β-Catenin (β-Catenin^{stab}) and KRAS^{G12V} (Fig. 5A). We detected increased and regional ERK phosphorylation in the proliferative zone, but not in differentiated enterocytes, following KRAS^{G12V} activation, which agrees with our reporter and transcriptome analyses. The increased ERK phosphorylation did not extend into the crypt bases, likely due to lower levels of transgene induction (see tdTomato staining in Fig. 5A, lower panels). Again, some enterocytes at the tip of the villus were strongly p-ERK-positive regardless of KRAS^{G12V} induction, confirming our findings of isolated p-ERK-positive late-stage enterocytes in the previous assays. Interestingly, we also detected increased p-ERK levels in the proliferative zone of transgenic mice producing β-Catenin^{stab}. However, only in mice with a double KRAS^{G12V}-β-Catenin^{stab}-encoding transgene, we observed many p-ERK-positive enterocytes throughout the villi. In contrast, we found that ERK phosphorylation depended on Wnt/β-Catenin activity in organoids, since removal of the Wnt co-ligand R-Spondin from cultures reduced p-ERK levels within 24h (Fig. 5B).

We next assessed KRAS^{G12V}-dependent proliferation and ERK phosphorylation in spheroid cells that have undergone a switch to an adenoma-like phenotype after long-term activation of stabilized β-Catenin and removal of the Wnt co-ligand R-Spondin (Fig. 5C-E). These cells largely phenocopy adenoma of the conventional CRC progression pathway, i.e. an early stage in tumour evolution after activation of the Wnt/β-Catenin pathway, but before mutational MAPK activation [40]. We found that adenomatous spheroids proliferate in the absence of EGF in the culture medium over several passages, regardless of whether they express a transgene encoding β-Catenin^{stab}, or a transgene encoding both β-Catenin^{stab} and KRAS^{G12V}. To test for self-sufficiency of spheroid proliferation, we used the EGFR inhibitor Gefitinib [41] to suppress residual autocrine or paracrine EGFR signals. Under these conditions, the growth of β-Catenin^{stab}-induced spheroid cultures stalled, while combined β-Catenin^{stab}- and KRAS^{G12V}-cultures maintained proliferation (Fig. 5B, C). This observation contrasted with organoids derived from normal intestinal tissue (that is, without long-term induction a β-Catenin^{stab} transgene), which were highly EGF dependent and could not employ KRAS^{G12V} to sustain proliferation (Supplementary Fig. 6). In contrast to our finding of increased ERK phosphorylation after β-Catenin activation in normal tissue, p-ERK levels were lower in adenomatous spheroids compared to normal tissue organoids (Fig. 5E). These experiments indicate that functional interactions between the Wnt/β-Catenin and MAPK pathways in the intestine may be different in normal and adenomatous tissue.

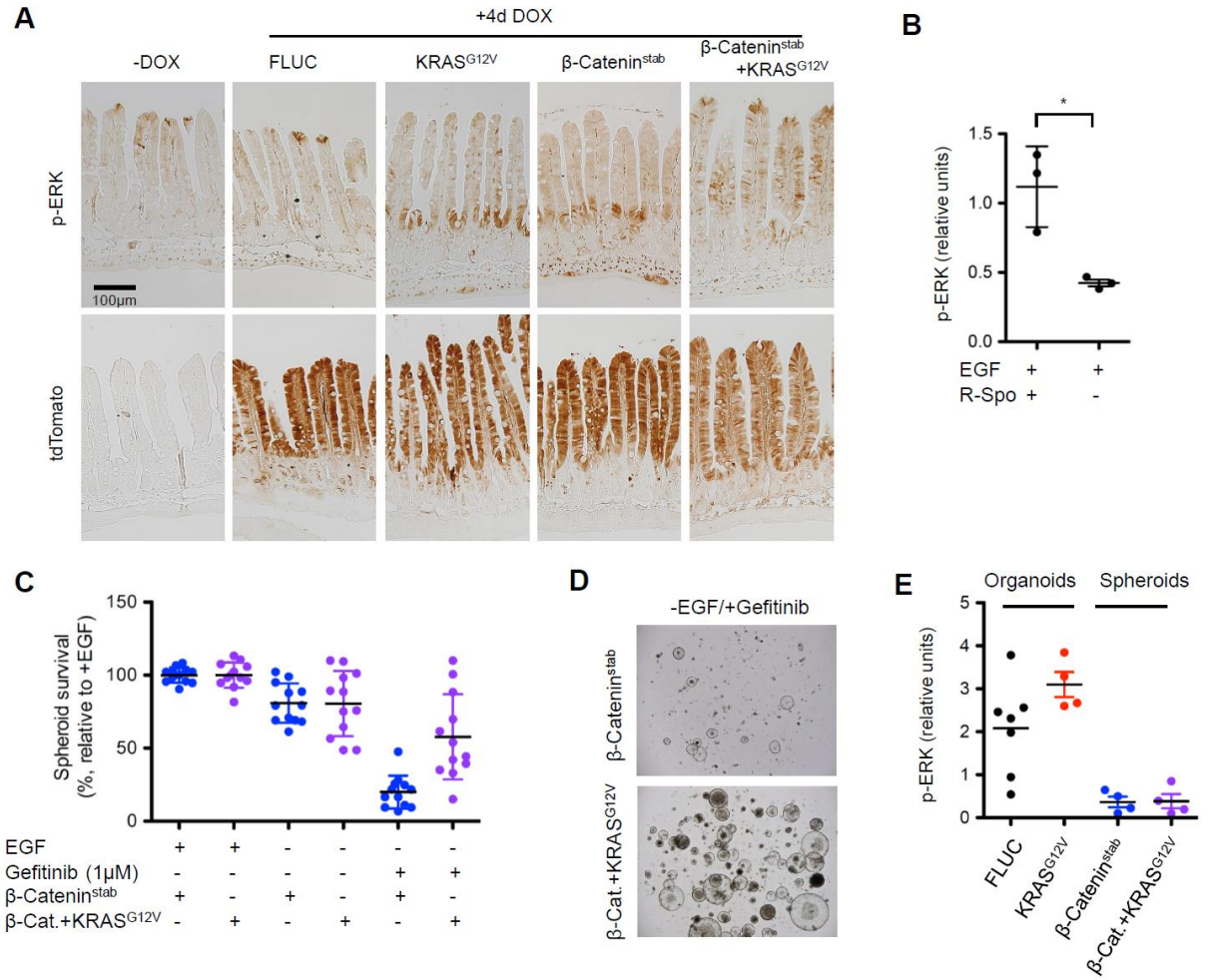

Figure 5: β-Catenin modulates ERK activity in intestinal cells A) Immunohistochemistry for phospho-ERK and tdTomato in intestines of transgenic mice, as indicated. B) Capillary protein quantification for phospho-ERK in intestinal organoids, 24 h after removal of the Wnt/β-Catenin co-activator R-Spondin. Triplicate assays are shown (p=0.014). C)-E) Proliferation of adenomatous spheroid after EGF depletion, EGFR inhibition by Gefitinib and/or $KRAS^{G12V}$ induction, 6 d after passaging. C) Quantification from multiple wells of 3 independent experiments, D) Representative images of β-$Catenin^{stab}$- or β-$Catenin^{stab}$/$KRAS^{G12}$ double transgenic spheroid cultures, 6 d after passaging and in the presence of 1 µM Gefitinib. E) phospho-ERK quantification in organoids and spheroids, using capillary protein analysis.

Dosage- and cell type-dependence of ERK phosphorylation in response to $KRAS^{G12V}$ in CRC cell lines

Our data indicate that signals transduced from KRAS to ERK are context dependent and thus may be subject to adaptation during CRC progression. To test this hypothesis, we compared ERK

phosphorylation in response to KRAS^{G12V} or BRAF^{V600E} in two CRC cell lines that have no mutations in KRAS, NRAS or BRAF. For this, SW48 and Caco2 cells were transfected with inducible expression vectors for tdTomato-KRAS^{G12V}, -BRAF^{V600E}, or -FLUC control, as previously used in the organoid cultures. 24h after induction, cells were fixed and oncogene levels, as extrapolated from tdTomato, and phosphorylation of ERK were measured via flow cytometry (Fig. 6A). We found that even low levels of BRAF^{V600E} strongly increased ERK phosphorylation in both cell lines. In contrast, the ability of KRAS^{G12V} to induce ERK phosphorylation was markedly different (Fig. 6B). In Caco2 cells, ERK phosphorylation increased step-wisely with KRAS^{G12V}-associated fluorescence, whereas in SW48 even high levels of transgenic tdTomato-KRAS^{G12V} were unable to induce strong ERK phosphorylation.

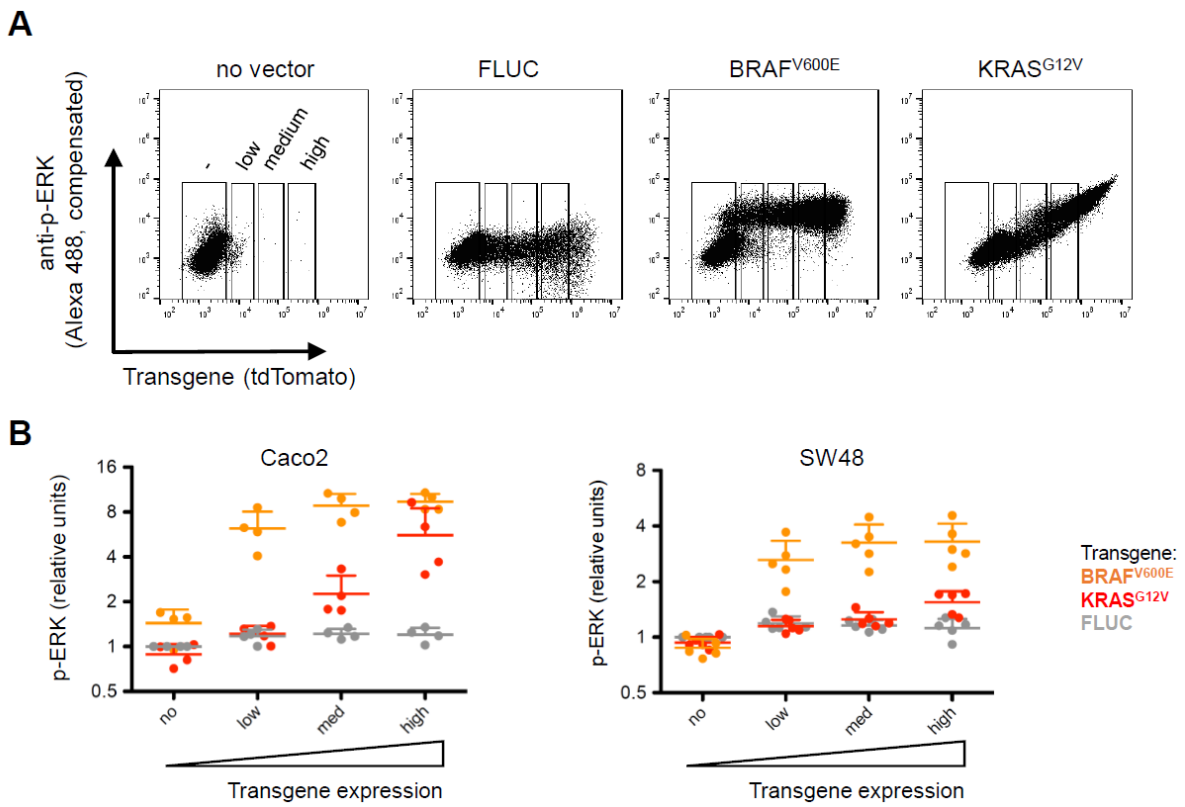

Figure 6: Oncogenic MAPK signal transduction differs between CRC cell lines A) Representative example of phospho-ERK regulation in Caco2 cells after transfection with tdTomato-KRAS^{G12V}-, -BRAF^{V600E} or -FLUC vectors, by flow cytometry. Gates along the x-axis categorize cells according to transgene dose, as used in B). B) Quantification of phospho-ERK in KRAS^{G12V}-, BRAF^{V600E}- or FLUC-transfected Caco2 and SW48 CRC cells, by flow cytometry. Mean and standard deviation of 4 or 5 independent replicate experiments is given. Grey: FLUC-; orange: BRAF^{V600E}; red: KRAS^{G12V}-transfected cells.

Discussion

By combining reporter assays and single cell RNA sequencing in transgenic intestinal organoids, we demonstrate that phosphorylation of ERK, the terminal kinase of the MAPK module, is regulated in a differential and cell typic-specific manner in response to $KRAS^{G12V}$ or $BRAF^{V600E}$. Both oncogenes therefore also differed in their abilities to induce cancer-associated phenotypes, such as loss of epithelial integrity and cell proliferation.

Importantly, we found that the ability of $KRAS^{G12V}$ to activate ERK was cell type-specific within the intestinal epithelium and divergent between CRC cell lines. This unexpected heterogeneity in MAPK signal transduction extends our understanding of how mutated KRAS, the most prevalent oncogene in CRC, exerts its effects. Importantly, local differences of ERK activity have recently been found in clinical specimens of CRC, including in KRAS-mutant CRC [15]. ERK levels were generally higher in cancer cells adjacent to stromal cells at the invasive front, and lower in more central areas of the cancer specimen, in line with modulation of ERK activity by cues from the microenvironment. Our results agree with the view of a dynamic MAPK pathway in the presence of oncogenic KRAS. However, we find here that ERK activity was turned off in differentiated enterocytes in organoid culture, even in the presence of extracellular EGF. Therefore, ERK activity in the presence of oncogenic KRAS can be regulated by both, external signals received from the microenvironment and intrinsic cellular differentiation states.

We found that Paneth cells and enterocytes represent main differentiated cell types of the intestinal epithelium with marked differences in their abilities to activate ERK following oncogenic activation of KRAS. It is of note that the former reside in the crypt compartment with high Wnt/β-Catenin activity, while the latter inhabit the villus with low β-Catenin activity. We therefore suggest that Wnt/β-Catenin is among the signals in the microenvironment that could regulate ERK activity in the intestine and in CRC. Indeed, a functional role for Wnt/β-Catenin in the activation of ERK in the intestinal epithelium has been proposed before [43].

We found that $KRAS^{G12V}$ cooperated with oncogenic β-Catenin in the induction of ERK activity, and that ERK activity in the normal intestine was reduced after removal of the Wnt/β-Catenin co-activator R-Spondin. Spheroid cells resembling intestinal adenoma were rendered EGF-independent by $KRAS^{G12V}$ induction, in contrast to normal mouse intestinal epithelium, where $KRAS^{G12V}$ was not sufficient to support proliferation. These findings could explain why oncogenic KRAS cannot initiate tumour development in the intestine, but nevertheless is the most frequent oncogenic event immediately after activation of Wnt/β-Catenin in the conventional tumour progression route leading

to CRC [9,10]. In this model, oncogenic KRAS provides sufficient pro-proliferative ERK activity only after β-Catenin activation, such as by the loss of the tumour suppressor APC.

In our experiments, signal transduction from BRAF to ERK was independent of cellular context. Extending previous studies [27,28], we found that high levels of MAPK induced by oncogenic $BRAF^{V600E}$ are not tolerated in the intestinal epithelium. This is in contrast to CRC and cell lines, where $BRAF^{V600E}$ amplifications exist and are selected for by MEK inhibition [44,45]. It thus appears that the corridor for acceptable MAPK activity is tuneable during CRC progression and under selective pressure exerted, for instance, by targeted therapy. Therefore, our findings are reminiscent of the "just right" signalling model that has been proposed to explain step-wise increases of β-Catenin activity in CRC progression [46].

We found that Caco2 cells phosphorylated ERK stepwisely when induced with increasing doses of $KRAS^{G12V}$, while no such response was observed in SW48 cells. This suggests that subgroups of CRC could differ in their regulation of ERK activity, even when harbouring the same oncogene in the MAPK pathway. This finding could explain part of the heterogeneity observed in response to anti-EGFR-therapy in the clinic, even after stratification of patients for mutations in KRAS, NRAS and BRAF [13]. Furthermore, we found that the cellular differentiation state and activity of Wnt/β-Catenin could modulate ERK phosphorylation and the ERK-dependent proliferative response in intestinal cells. Our findings thus suggest that controlling cellular differentiation or targeting morphogenetic signalling pathways such as Wnt/β-Catenin could represent a means to inhibit oncogenic MAPK activity in subgroups of KRAS/BRAF-wildtype and KRAS-mutant, but not in BRAF-mutant CRCs.

Materials and Methods

Generation of transgenic mice

Transgene cassettes were constructed by linking tdTomato to human BRAF(V600E), KRAS(G12V) and/or murine stabilized mutant Ctnnb1 (S33A, S37A, T41A, S45A) or firefly luciferase via 2A peptides, and subsequent cloning of these gene combinations into a doxycycline-inducible expression cassette flanked by heterologous loxP sites, and integrated into a previously modified Gt(ROSA)26Sor locus of F1 hybrid B6/129S6 embryonic stem cells by Cre recombinase-mediated cassette exchange, as described previously [26]. Transgenic animal production was approved by Berlin authorities LAGeSo (G0185/09, G0143/14).

Cell and Organoid culture and protein analysis

Organoid cultures were initiated and propagated as described before [25], using 48-well plates with 15 µl droplets of Matrigel (Corning) per well overlaid with 300 µl crypt culture medium containing EGF (50 ng/ml), Noggin (100 ng/ml) and R-Spondin1 (functionally tested from R-Spondin-conditioned medium; CCM-REN). Transgenes were induced by addition of 2 µg/ml doxycycline to the medium. For spheroid cultures, R-Spondin was removed after induction of a transgene endoding β-Catenin^{stab} alone or in combination with KRAS^{G12V}. During passaging, spheroids were dissociated with TrypLE (Gibco) for 3 min and Rho kinase inhibitor Y27632 (10 µM) was added to the culture medium to prevent anoikis. The following inhibitors (SelleckChem) were employed: AZD6244 (10 µM), BVD-523 (3 µM), AZD8931 (50 nm), Gefitinib (1 µm).

Organoid and spheroid survival was scored as follows: cultures were passaged, inhibitors and doxycycline were applied to the culture medium directly after passaging. Individual wells were imaged using the z-stack function of Biozero observation and analyser software (Keyence) on day 1 and 4 (organoids) or day 1 and 6 (spheroids), and full focus-reconstructed images were used for quantification.

For viral transfection, a protocol from reference [48] was employed, with modifications: organoids were cultured in the presence of Y27632 and the GSK3β inhibitor CHIR99021 for two days. Next, organoids were disaggregated into single cells using TrypLE (Gibco) for 5min. at 37°C. Cell suspensions were spin-oculated in an ultra-low adhesion round bottom 96-well plate with the virus at 300 g for 45min. Subsequently, cells were resuspended in Matrigel, and cultured for 2 days in CCM-REN supplemented with Y27632 and CHIR99021. Subsequently, medium was replaced by CCM-REN containing 2 µg/ml Puromycin to select for transfected cells. As viral transfection initially resulted in organoid pools that were heterogeneous for FIRE reporter activity, single FIRE positive organoids were manually selected and propagated before experimental analysis.

Protein sample preparation and quantification of pERK was performed as previously described [47] using a WES capillary system (12–230 kD Master kit α-Rabbit–HRP; PS-MK01; Protein Simple) and the antibody pERK/2(T202/Y204) (1:50; #9101, Cell Signal). Raw pERK values were normalized to vinculin (1:30; #4650; Cell Signal).

Immunohistochemistry was done on paraformaldehyde fixed and paraffin-embedded tissues. Organoids were fixed in 4% paraformaldehyde for 30 minutes, while intestines were fixed over night at room temperature. Subsequently, tissues were dehydrated in a graded ethanol series, followed by xylene. Tissues were paraffine-embedded, sectioned at 4µm and mounted on Superfrost Plus slides (Thermo Fisher Scientific). Sections were deparaffinised, rehydrated, bleached for 10 min. in 3% H_2O_2. Antigens were retrieved using 10mM Na-citrate, pH 6 for 20 minutes at boiling temperature. The following antibodies were used: Phospho-ERK (T202/Y204; #4370 Cell Signal); anti-RFP (1:200; #600-401-379 Rockland). ImmPRESS secondary antibody and NovaRED substrate kits (Vector Labs) were used for signal detection, according to manufacturer´s protocols.

SW48 and Caco2 CRC cells were cultured in L-15 and DMEM, respectively, supplemented with 10% fetal bovine serum. Cells were transfected using Lipofectamin 3000 Transfection Reagent (Thermo Fischer) with vectors encoding $BRAF^{V600E}$, $KRAS^{G12V}$ or FLUC linked to tdTomato and the pTet-on Advanced Vector (Clontech). Cells were starved in medium containing 0.1%fetal bovine serum and induced with 2 µg/ml doxycycline 48h after transfection. 24 h later, cells were harvested using TrypLE, washed, rested for 30 min at 37°C in starvation medium and fixed in 4% PFA for 15 min. at 37°C. Fixed cells were washed in PBS/1% BSA, permeabilised in MeOH at -20°C overnight, and immunostained with Alexa Fluor 488 mouse anti-ERK1/2 (pT202/pY204) antibody (1:10; 612592, BD Bioscience) for 30 min.

Immunofluorescence and microscopy

For immunofluorescence imaging, organoids were washed with PBS and fixed in-well with 4% paraformaldehyde (PFA) for 30 min at 37°C. Fixation was stopped with PBS containing 100 nm Glycine. Cells were blocked and permeabilised with blocking buffer (PBS containing 1% BSA, 0.2 % Triton X100, 0.05 % Tween-20) for at least 2.5 h at room temperature. Samples were incubated for 36 h at 4°C with primary antibodies against lysozyme (1:250; ab108508, Abcam) or Ki-67 (1:100, PA5-16785, Invitrogen) diluted in blocking buffer. After washing with IF-buffer (PBS containing 0.1% BSA, 0.2 % Triton X100, 0.05 % Tween-20), samples were incubated for 24h at 4°C with secondary antibody Alexa Fluor 647 anti-rabbit (1:500, #4414, Molecular Probes) diluted in IF-buffer. Samples were counterstained for 5 min at room temperature using 0.5 µg/ml DAPI. After washing with IF-buffer, stained cultures were released from the Matrigel and collected in PBS. Samples were washed,

resuspended in remaining PBS and mounted on slides using Vectashield Antifade Mounting Medium (H-1000, Vector).

Immunofluorescence and FIRE reporter images were taken with a Leica TSC SPE confocal microscope using an ACS 20x oil-immersion objective, solid-state lasers (405, 488, 532 and 635 nm) as sources of excitation and LAS X operating software (Leica). Light microscopy images of cultures were taken with a Biozero microscope using a Plan Apo 4x NA 0.20 objective and Biozero observation and analyser software (Keyence).

For transmission electron microscopy, organoids were induced for 24 h, removed from Matrigel and fixed in a buffer containing 2% paraformaldehyde and 2.5% glutaraldehyde at 4°C. Regions of approximately 100-150 μm^2 showing representative sections through organoids were imaged on a 120 kV Tecnai Spirit transmission electron microscope (FEI) equipped with a F416 CMOS camera (TVIPS). Micrographs were recorded automatically at a final magnification of 4400x (2.49 nm pixel size at object scale) and -10 µm defocus using Leginon [49] and then stitched using TrakEM2 [50].

Flow cytometry and Fluorescence-activated cell sorting

Flow cytometry of α-pERK-stained CRC cells resuspended in PBS/1%BSA cells was done using an Accuri cytometer (BD). Cells were gated for populations displaying different tdTomato fluorescence values (negative, low, medium and high), which correlates with transgene expression. For each population, the mean α-pERK fluorescence values were determined and normalised to the tdTomato negative fraction of the corresponding FLUC control experiment.

For fluorescence-activated cell sorting of organoid cells, single cell suspensions from induced organoids were prepared by digestion with TrypLE (Thermo Fisher Scientific) in the presence of 2 mM EDTA and 200 u/ml DNAse I. Digestion was monitored by visual inspection, and stopped by crypt culture medium containing 0.2% bovine serum albumin. Cell suspensions were filtered through 30 µm Celltrix filters and stained with an anti-CD44-antibody conjugated to Allophycocyanin (APC; clone IM7, BioLegend) and the Green or Near-IR Live/Dead Fixable Dead Cell Stain Kits (Life Tech) for subsequent exclusion of dead cells. Single cells were sorted into the 96-well plates of the Precise WTA Kit (BD) with pre-dispensed library chemistry using a BD FACSAriaII SORP (BD) and a gating strategy as displayed in Supplementary Figure 3. Cells were sorted into quadrants of plates to minimize batch effects between plates. For later analysis of CD44 positivity of the subsets, sorts were performed as index sorts.

RNA sequencing and bioinformatic analyses

For single cell RNA sequencing, the Precise WTA Kit (BD) was used, according to the manufacturers´ instructions. Sequences were produced using NextSeq and/or HiSeq chemistry (Illumina). Cluster generation on NextSeq 500 followed the instructions of the manufacturer, at a final loading concentration of 2 pM on a High-Output-Flowcell. 1% PhiX was added as quality control, at least $4x10^7$ paired reads per pool were gained during a Paired-End-75 run. Library-pools running on the HiSeq4000-system were prepared according to Illumina recommendations, loaded with 200 pM and sequenced during a Paired-End-75 run. Again, 1% PhiX was added as quality control, and at least $4x10^7$ read-pairs per pool were targeted.

Single cell RNA-sequencing data was pre-processed using the BD Precise Whole Transcriptome Assay Analysis Pipeline v2.0 [51]. Quality control was performed using scater [52]. Read counts were normalised using the trimmed mean of median values (TMM) approach provided with edgeR [53]. Normalised read counts were used for k-means clustering and t-SNE visualisation. Differentiation trajectories in t-SNE plots were determined using slingshot [54], with intestinal stem cell cluster 1 as predefined origin. Differentially expressed genes were called on log-transformed raw counts using a hurdle model provided with R package MAST [55]. Top-10 signature genes per cluster were identified by comparing average gene expressions within cluster to average gene expressions across all other clusters. For bulk cell RNA sequencing, organoids were induced for 24 h with 2 µg/ml doxycycline in CCM-REN medium and subsequently dissociated, as described before [47]. RNA-seq reads were aligned to the mouse genome GRCm38 using STAR aligner with GENCODE annotation vM11. Differentially expressed genes were called using DESeq2. scRNA-seq and bulk RNA-seq data are available in the GEO repository under accession numbers GSE115242 and GSE115234, respectively.

Statistics

Error bars in figures denote standard deviations. p-values are calculated form two-tailed unpaired t-tests in GraphPad prism. *, ** and *** denote p-values <0.05, <0.01 and <0.001, respectively.

Acknowledgements

The authors gratefully acknowledge excellent technical assistance by Gaby Blaess and Sonja Banko (MPIMG, Berlin) for mouse genotyping and mouse care, respectively. The authors are also gratefully acknowledge the help of lab students Ekaterina Eroshok and Maximilian Anders (Molecular Medicine Masters´ programme, Charité – Universitätsmedizin Berlin) with immunohistochemistry in the early phase of this project. We received the FIRE plasmid as a kind gift from John Albeck, UC Davis.

Funding

The work was in part funded by Deutsche Forschungsgemeinschaft (Grant MO2783/2-1 to MM), Berlin School of Integrative Oncology (starter grant to NB and MM), and the German Cancer Consortium DKTK (single cell grant to NB and MM).

Author contributions

RB, PR, CG, SiS, NM, BF, IAES conducted, analysed, and interpreted experiments; FU performed bioinformatic analyses; PR, TM, BGH, CS, NB, MM conceived, designed, interpreted experiments and/or supervised parts of the study; MM wrote the manuscript.

Conflict of interest

The authors declare that they have no conflict of interest.

References

1. Beumer J, Clevers H (2016) Regulation and plasticity of intestinal stem cells during homeostasis and regeneration. *Development* **143**: 3639–3649.

2. Stelniec-Klotz I, Legewie S, Tchernitsa O, Witzel F, Klinger B, Sers C, Herzel H, Blüthgen N, Schäfer R (2012) Reverse engineering a hierarchical regulatory network downstream of oncogenic KRAS. *Mol Syst Biol* **8**: 601.

3. Sasaki N, Sachs N, Wiebrands K, Ellenbroek SIJ, Fumagalli A, Lyubimova A, Begthel H, van den Born M, van Es JH, Karthaus WR, et al. (2016) Reg4 $^{+}$ deep crypt secretory cells function as epithelial niche for Lgr5 $^{+}$ stem cells in colon. *Proc Natl Acad Sci* **113**: E5399–E5407.

4. Sato T, van Es JH, Snippert HJ, Stange DE, Vries RG, van den Born M, Barker N, Shroyer NF, van de Wetering M, Clevers H (2011) Paneth cells constitute the niche for Lgr5 stem cells in intestinal crypts. *Nature* **469**: 415–418.

5. Pylayeva-Gupta Y, Grabocka E, Bar-Sagi D (2011) RAS oncogenes: weaving a tumorigenic web. *Nat Rev Cancer* **11**: 761–774.

6. Holderfield M, Deuker MM, McCormick F, McMahon M (2014) Targeting RAF kinases for cancer therapy: BRAF-mutated melanoma and beyond. *Nat Rev Cancer* **14**: 455–467.

7. Ciardiello F, Kim N, Saeki T, Dono R, Persico MG, Plowman GD, Garrigues J, Radke S, Todaro GJ, Salomon DS (1991) Differential expression of epidermal growth factor-related proteins in human colorectal tumors. *Proc Natl Acad Sci U S A* **88**: 7792–7796.

8. Papke B, Der CJ (2017) Drugging RAS: Know the enemy. *Science (80-)* **355**: 1158–1163.

9. Fearon ER, Vogelstein B (1990) A genetic model for colorectal tumorigenesis. *Cell* **61**: 759–767.

10. Fearon ER (2011) Molecular genetics of colorectal cancer. *Annu Rev Pathol* **6**: 479–507.

11. Rad R, Cadiñanos J, Rad L, Varela I, Strong A, Kriegl L, Constantino-Casas F, Eser S, Hieber M, Seidler B, et al. (2013) A Genetic Progression Model of Braf(V600E)-Induced Intestinal Tumorigenesis Reveals Targets for Therapeutic Intervention. *Cancer Cell* **24**: 15–29.

12. Yachida S, Mudali S, Martin SA, Montgomery EA, Iacobuzio-Donahue CA (2009) Beta-catenin nuclear labeling is a common feature of sessile serrated adenomas and correlates with early neoplastic progression after BRAF activation. *Am J Surg Pathol* **33**: 1823–1832.

13. Morkel M, Riemer P, Bläker H, Sers C (2015) Similar but different: distinct roles for KRAS and

BRAF oncogenes in colorectal cancer development and therapy resistance. *Oncotarget* **6**: 20785–20800.

14. Blaj C, Schmidt EM, Lamprecht S, Hermeking H, Jung A, Kirchner T, Horst D (2017) Oncogenic effects of high MAPK activity in colorectal cancer mark progenitor cells and persist irrespective of RAS mutations. *Cancer Res* **77**: 1763–1774.

15. Hlubek F, Brabletz T, Budczies J, Pfeiffer S, Jung A, Kirchner T (2007) Heterogeneous expression of Wnt/beta-catenin target genes within colorectal cancer. *Int J cancer J Int du cancer* **121**: 1941–1948.

16. Snippert HJ, van Es JH, van den Born M, Begthel H, Stange DE, Barker N, Clevers H (2009) Prominin-1/CD133 marks stem cells and early progenitors in mouse small intestine. *Gastroenterology* **136**: 2187–2194.e1.

17. Zhu L, Gibson P, Currle DS, Tong Y, Richardson RJ, Bayazitov IT, Poppleton H, Zakharenko S, Ellison DW, Gilbertson RJ (2009) Prominin 1 marks intestinal stem cells that are susceptible to neoplastic transformation. *Nature* **457**: 603–607.

18. O'Brien CA, Pollett A, Gallinger S, Dick JE (2007) A human colon cancer cell capable of initiating tumour growth in immunodeficient mice. *Nature* **445**: 106–110.

19. Todaro M, Alea MP, Di Stefano AB, Cammareri P, Vermeulen L, Iovino F, Tripodo C, Russo A, Gulotta G, Medema JP, et al. (2007) Colon cancer stem cells dictate tumor growth and resist cell death by production of interleukin-4. *Cell Stem Cell* **1**: 389–402.

20. Sadanandam A, Lyssiotis CA, Homicsko K, Collisson EA, Gibb WJ, Wullschleger S, Ostos LCG, Lannon WA, Grotzinger C, Del Rio M, et al. (2013) A colorectal cancer classification system that associates cellular phenotype and responses to therapy. *Nat Med* **19**: 619–625.

21. Kreso A, O'Brien CA, Van Galen P, Gan OI, Notta F, Brown AMK, Ng K, Jing M, Wienholds E, Dunant C, et al. (2013) Variable clonal repopulation dynamics influence chemotherapy response in colorectal cancer. *Science (80-)* **339**: 543–548.

22. Albeck JG, Mills GB, Brugge JS (2013) Frequency-Modulated Pulses of ERK Activity Transmit Quantitative Proliferation Signals. *Mol Cell* **49**: 249–261.

23. Grün D, Lyubimova A, Kester L, Wiebrands K, Basak O, Sasaki N, Clevers H, van Oudenaarden A (2015) Single-cell messenger RNA sequencing reveals rare intestinal cell types. *Nature* **525**: 251–255.

24. Li H, Courtois ET, Sengupta D, Tan Y, Chen KH, Goh JJL, Kong SL, Chua C, Hon LK, Tan WS, et al.

(2017) Reference component analysis of single-cell transcriptomes elucidates cellular heterogeneity in human colorectal tumors. *Nat Genet* **49**: 708–718.

25. Sato T, Vries RG, Snippert HJ, van de Wetering M, Barker N, Stange DE, van Es JH, Abo A, Kujala P, Peters PJ, et al. (2009) Single Lgr5 stem cells build crypt-villus structures in vitro without a mesenchymal niche. *Nature* **459**: 262–265.

26. Vidigal JA, Morkel M, Wittler L, Brouwer-Lehmitz A, Grote P, Macura K, Herrmann BG (2010) An inducible RNA interference system for the functional dissection of mouse embryogenesis. *Nucleic Acids Res* **38**: e122.

27. Riemer P, Sreekumar A, Reinke S, Rad R, Schäfer R, Sers C, Bläker H, Herrmann BG, Morkel M (2015) Transgenic expression of oncogenic BRAF induces loss of stem cells in the mouse intestine, which is antagonized by β-catenin activity. *Oncogene* **34**: 3164–3175.

28. Tong K, Pellón-Cárdenas O, Sirihorachai VR, Warder BN, Kothari OA, Perekatt AO, Fokas EE, Fullem RL, Zhou A, Thackray JK, et al. (2017) Degree of Tissue Differentiation Dictates Susceptibility to BRAF-Driven Colorectal Cancer. *Cell Rep* **21**: 3833–3845.

29. Yeh TC, Marsh V, Bernat BA, Ballard J, Colwell H, Evans RJ, Parry J, Smith D, Brandhuber BJ, Gross S, et al. (2007) Biological characterization of ARRY-142886 (AZD6244), a potent, highly selective mitogen-activated protein kinase kinase 1/2 inhibitor. *Clin Cancer Res* **13**: 1576–1583.

30. Sullivan RJ, Infante JR, Janku F, Lee Wong DJ, Sosman JA, Keedy V, Patel MR, Shapiro GI, Mier JW, Tolcher AW, et al. (2018) First-in-class ERK1/2 inhibitor ulixertinib (BVD-523) in patients with MAPK mutant advanced solid tumors: Results of a phase I dose-escalation and expansion study. *Cancer Discov* **8**: 184–195.

31. Barlaam B, Anderton J, Ballard P, Bradbury RH, Hennequin LFA, Hickinson DM, Kettle JG, Kirk G, Klinowska T, Lambert-Van Der Brempt C, et al. (2013) Discovery of AZD8931, an equipotent, reversible inhibitor of signaling by EGFR, HER2, and HER3 receptors. *ACS Med Chem Lett* **4**: 742–746.

32. Uhlitz F, Sieber A, Wyler E, Fritsche-Guenther R, Meisig J, Landthaler M, Klinger B, Blüthgen N (2017) An immediate–late gene expression module decodes ERK signal duration. *Mol Syst Biol* **13**: 928.

33. Wang F, Scoville D, He XC, Mahe MM, Box A, Perry JM, Smith NR, Lei NY, Davies PS, Fuller MK, et al. (2013) Isolation and characterization of intestinal stem cells based on surface marker

combinations and colony-formation assay. *Gastroenterology* **145**:.

34. Merlos-Suárez A, Barriga FM, Jung P, Iglesias M, Céspedes MV, Rossell D, Sevillano M, Hernando-Momblona X, da Silva-Diz V, Muñoz P, et al. (2011) The intestinal stem cell signature identifies colorectal cancer stem cells and predicts disease relapse. *Cell Stem Cell* **8**: 511–524.

35. Sato T, van Es JH, Snippert HJ, Stange DE, Vries RG, van den Born M, Barker N, Shroyer NF, van de Wetering M, Clevers H (2010) Paneth cells constitute the niche for Lgr5 stem cells in intestinal crypts. *Nature* **469**: 415.

36. Gonzalo DH, Lai KK, Shadrach B, Goldblum JR, Bennett AE, Downs-Kelly E, Liu X, Henricks W, Patil DT, Carver P, et al. (2013) Gene expression profiling of serrated polyps identifies annexin A10 as a marker of a sessile serrated adenoma/polyp. *J Pathol* **230**: 420–429.

37. Peeters T, Vantrappen G (1975) The Paneth cell: a source of intestinal lysozyme. *Gut* **16**: 553–558.

38. Simmons AJ, Banerjee A, McKinley ET, Scurrah CR, Herring CA, Gewin LS, Masuzaki R, Karp SJ, Franklin JL, Gerdes MJ, et al. (2015) Cytometry-based single-cell analysis of intact epithelial signaling reveals MAPK activation divergent from TNF- -induced apoptosis in vivo. *Mol Syst Biol* **11**: 835–835.

39. van der Flier LG, Clevers H (2009) Stem cells, self-renewal, and differentiation in the intestinal epithelium. *Annu Rev Physiol* **71**: 241–260.

40. Farrall AL, Riemer P, Leushacke M, Sreekumar A, Grimm C, Herrmann BG, Morkel M (2012) Wnt and BMP signals control intestinal adenoma cell fates. *Int J cancer J Int du cancer* **131**: 2242–2252.

41. Wakeling A, Guy S, Woodburn J (2002) ZD1839 (Iressa) an orally active inhibitor of epidermal growth factor signaling with potential for cancer therapy. *Cancer Res* **1839**: 5749–5754.

42. Young A, Lou D, McCormick F (2013) Oncogenic and wild-type ras play divergent roles in the regulation of mitogen-activated protein kinase signaling. *Cancer Discov* **3**: 113–123.

43. Phelps RA, Chidester S, Dehghanizadeh S, Phelps J, Sandoval IT, Rai K, Broadbent T, Sarkar S, Burt RW, Jones DA (2009) A Two-Step Model for Colon Adenoma Initiation and Progression Caused by APC Loss. *Cell* **137**: 623–634.

44. Corcoran RB, Dias-Santagata D, Bergethon K, Iafrate AJ, Settleman J, Engelman JA (2010) BRAF gene amplification can promote acquired resistance to MEK inhibitors in cancer cells

harboring the BRAF V600E mutation. *Sci Signal* **3**: ra84.

45. Little AS, Balmanno K, Sale MJ, Newman S, Dry JR, Hampson M, Edwards PAW, Smith PD, Cook SJ (2011) Amplification of the driving oncogene, KRAS or BRAF, underpins acquired resistance to MEK1/2 inhibitors in colorectal cancer cells. *Sci Signal* **4**: ra17.

46. Albuquerque C, Breukel C, van der Luijt R, Fidalgo P, Lage P, Slors FJM, Leitão CN, Fodde R, Smits R (2002) The 'just-right' signaling model: APC somatic mutations are selected based on a specific level of activation of the beta-catenin signaling cascade. *Hum Mol Genet* **11**: 1549–1560.

47. Riemer P, Rydenfelt M, Marks M, van Eunen K, Thedieck K, Herrmann BG, Blüthgen N, Sers C, Morkel M (2017) Oncogenic β-catenin and PIK3CA instruct network states and cancer phenotypes in intestinal organoids. *J Cell Biol* **216**: 1567–1577.

48. Fujii M, Matano M, Nanki K, Sato T (2015) Efficient genetic engineering of human intestinal organoids using electroporation. *Nat Protoc* **10**: 1474–1485.

49. Suloway C, Pulokas J, Fellmann D, Cheng A, Guerra F, Quispe J, Stagg S, Potter CS, Carragher B (2005) Automated molecular microscopy: The new Leginon system. *J Struct Biol* **151**: 41–60.

50. Cardona A, Saalfeld S, Schindelin J, Arganda-Carreras I, Preibisch S, Longair M, Tomancak P, Hartenstein V, Douglas RJ (2012) TrakEM2 software for neural circuit reconstruction. *PLoS One* **7**:.

51. Fu GK, Wilhelmy J, Stern D, Fan HC, Fodor SPA (2014) Digital encoding of cellular mRNAs enabling precise and absolute gene expression measurement by single-molecule counting. *Anal Chem* **86**: 2867–2870.

52. McCarthy DJ, Campbell KR, Lun ATL, Wills QF (2017) Scater: Pre-processing, quality control, normalization and visualization of single-cell RNA-seq data in R. *Bioinformatics* **33**: 1179–1186.

53. Robinson MD, McCarthy DJ, Smyth GK (2010) edgeR: a Bioconductor package for differential expression analysis of digital gene expression data. *Bioinformatics* **26**: 139–140.

54. Street K, Risso D, Fletcher RB, Das D, Ngai J, Yosef N, Purdom E, Dudoit S (2017) Slingshot: Cell lineage and pseudotime inference for single-cell transcriptomics. *bioRxiv* 128843.

55. Finak G, McDavid A, Yajima M, Deng J, Gersuk V, Shalek AK, Slichter CK, Miller HW, McElrath MJ, Prlic M, et al. (2015) MAST: A flexible statistical framework for assessing transcriptional changes and characterizing heterogeneity in single-cell RNA sequencing data. *Genome Biol*

16:278.